

Crossover in domain wall potential polarity as a function of anti-notch geometry

This article has been downloaded from IOPscience. Please scroll down to see the full text article.

2011 J. Phys. D: Appl. Phys. 44 235002

(<http://iopscience.iop.org/0022-3727/44/23/235002>)

View [the table of contents for this issue](#), or go to the [journal homepage](#) for more

Download details:

IP Address: 155.69.203.1

The article was downloaded on 19/05/2011 at 02:41

Please note that [terms and conditions apply](#).

Crossover in domain wall potential polarity as a function of anti-notch geometry

M Chandra Sekhar, S Goolaup¹, I Purnama and W S Lew²

School of Physical and Mathematical Sciences, Nanyang Technological University, 21 Nanyang Link, Singapore 637371, Singapore

E-mail: wensiang@ntu.edu.sg

Received 7 January 2011, in final form 11 April 2011

Published 18 May 2011

Online at stacks.iop.org/JPhysD/44/235002

Abstract

We have carried out a systematic study on domain wall (DW) pinning at an anti-notch in a Ni₈₀Fe₂₀ nanowire. Micromagnetic studies reveal that the potential polarity experienced by the DW at the anti-notch is a function of both DW chirality and anti-notch geometry. A transition in the potential disruption experienced by the DW is observed when the anti-notch height-to-width ratio (H_{AN}/W_{AN}) is 2. This transition is due to the relative orientation of the spins in the anti-notch with respect to the transverse component of the DW. When the anti-notch acts as a potential barrier, the DW undergoes damped oscillations prior to coming to an equilibrium position. The equilibrium position is a strong function of the anti-notch dimensions when the H_{AN}/W_{AN} ratio < 2 and is constant for $H_{AN}/W_{AN} \geq 2$. The effect of the relative orientation between the spins in the anti-notch and the transverse component of the DW on the shape of the potential is discussed.

(Some figures in this article are in colour only in the electronic version)

1. Introduction

Current-driven domain wall (DW) motion due to the spin transfer torque effect in ferromagnetic nanowires has attracted considerable interest due to its promising applications in DW memory [1] and logic devices [2]. Following the prediction by Berger [3] the spin torque effect has been extensively studied both theoretically and experimentally. In ferromagnetic nanowires two types of DWs are stable: the transverse and vortex walls. The transverse DWs are stable in narrow nanowires [5, 6] and can be broadly classified as head to head (HH) and tail to tail (TT) [4] following their magnetization orientation. In HH configuration, the two magnetization components point to each other, and conversely for TT, the two components point in the opposite directions. In addition, the transverse DW possesses another degree of freedom, i.e. the transverse component of the DW which can either point upwards (HH-U) or downwards (HH-D), perpendicular to

the wire axis. Artificial defects are usually created in the ferromagnetic nanowires for introducing a potential energy landscape that can manipulate the motion of the DW. For memory applications it is imperative to understand the motion and pinning of the DW at the artificial defects, so that a total control of the DW motion in the nanowire structures can be obtained. Several studies have reported on the motion and pinning of the DW with notch and anti-notch defects [7–18]. Atkinson *et al* [8] showed that the pinning and depinning of the DWs depend on their micromagnetic configuration at a notch. Petit *et al* [9, 10] reported on the potential strengths and potential energy modifications of DW with different configurations at a T-shaped anti-notch. They showed that the potential as seen by the DW at a notch/anti-notch is a function of the DW configuration.

Recent studies on different notch geometries have shown that the potential strength as seen by the DW is a strong function of the shape and dimensions. However, the polarity of the potential does not change. In this work, we show that for an anti-notch geometry, a crossover in the potential polarity is observed as the anti-notch dimensions are varied. In

¹ Present address: Department of Electrical and Electronic Engineering, Faculty of Engineering, University of Mauritius, Reduit, Mauritius.

² Author to whom any correspondence should be addressed.

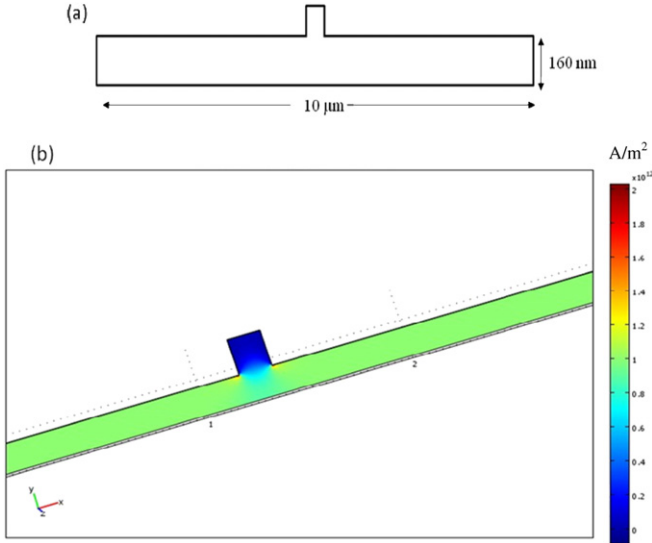


Figure 1. (a) Schematic diagram of the nanowire with an anti-notch at the centre. (b) Simulated current distribution through the nanowire with an anti-notch when the applied current density is 10^{12} A m^{-2} .

field-induced DW motion, the magnetization state at the anti-notch configuration is affected by the external driving magnetic field. For current-driven DW motion, the magnetization state of the anti-notch is not affected by the spin torque current. The crossover in the potential disruption is observed for the anti-notch when $H_{\text{AN}}/W_{\text{AN}}$ is 2. This is due to the variation in the magnetic charges at the anti-notch geometry. A potential barrier transition from smooth and gradual to abrupt and steep is observed as the $H_{\text{AN}}/W_{\text{AN}}$ ratio of the anti-notch is varied.

2. Micromagnetic simulation

In this study a $\text{Ni}_{80}\text{Fe}_{20}$ nanowire of length $10 \mu\text{m}$ and thickness 10 nm was considered. The chosen width of the nanowire was 160 nm in order to ensure that transverse DWs are the only stable DW configurations. To investigate the DW pinning, an anti-notch was introduced along the nanowire length. The anti-notch has a rectangular geometry with width W_{AN} and height H_{AN} . The notch was situated at the middle of the wire $5 \mu\text{m}$ from each edge as depicted in figure 1(a). The material parameters used in the simulation were saturation magnetization (M_s) = $800 \times 10^3 \text{ A m}^{-1}$, exchange stiffness constant (A_{ex}) = $1.3 \times 10^{-11} \text{ J m}^{-1}$ and magnetocrystalline anisotropy $k = 0$. We used the Object Oriented Micromagnetic Framework code (OOMMF) [19] extended by incorporating the spin transfer torque term [20] to the Landau–Lifshitz–Gilbert (LLG) equation to simulate the DW motion. The unit cell size for all simulations was set to be $5 \text{ nm} \times 5 \text{ nm} \times 5 \text{ nm}$. The LLG equation including the spin torque can be written as follows:

$$\frac{\partial \mathbf{M}(t)}{\partial t} = -\gamma_0 \mathbf{M} \times \mathbf{H}_{\text{eff}} + \frac{\alpha}{M_s} \mathbf{M} \times \frac{\partial \mathbf{M}(t)}{\partial t} - (\mathbf{u} \cdot \nabla) \mathbf{M} + \frac{\beta}{M_s} \mathbf{M} \times [(\mathbf{u} \cdot \nabla) \mathbf{M}]. \quad (1)$$

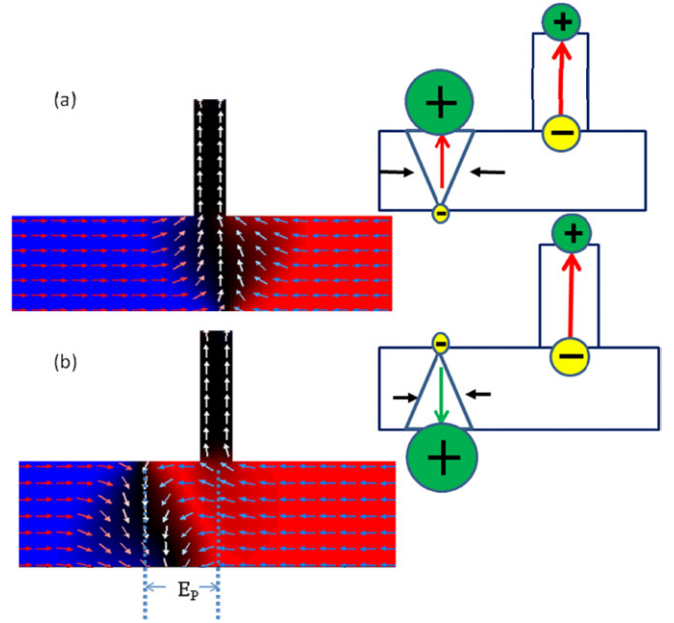


Figure 2. (a) Snap shot image of DW configuration of HH-U when it approaches an anti-notch of width $W_{\text{AN}} = 40 \text{ nm}$ and height $H_{\text{AN}} = 200 \text{ nm}$. (b) Snap shot image of DW configuration of HH-D when it approaches an anti-notch of width $W_{\text{AN}} = 40 \text{ nm}$ and height $H_{\text{AN}} = 200 \text{ nm}$.

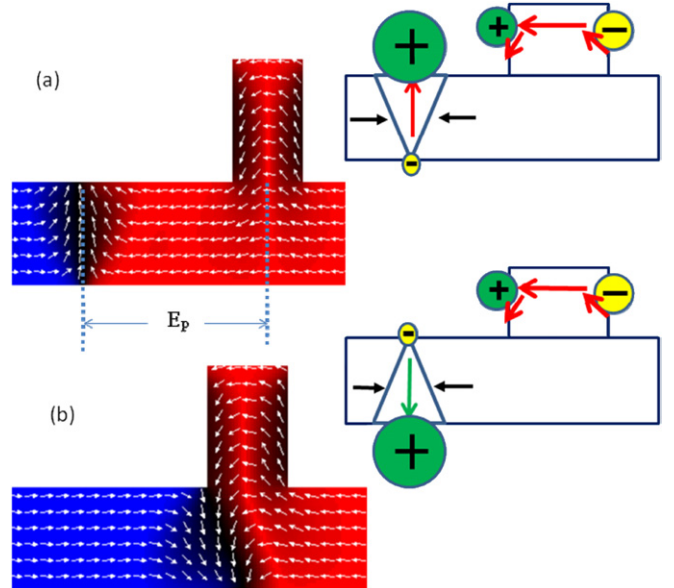


Figure 3. (a) Snap shot image of DW configuration of HH-U when it approaches an anti-notch of width $W_{\text{AN}} = 120 \text{ nm}$ and height $H_{\text{AN}} = 200 \text{ nm}$. (b) Snap shot image of DW configuration of HH-D when it approaches an anti-notch of width $W_{\text{AN}} = 120 \text{ nm}$ and height $H_{\text{AN}} = 200 \text{ nm}$.

The first term on the right-hand side in the equation relates to the torque exerted on the magnetization vector \mathbf{M} by the effective magnetic field \mathbf{H}_{eff} and the second term describes the Gilbert damping torque, parametrized by the Gilbert damping constant (α) which is fixed at 0.005 in our simulations. The last two terms are the spin transfer torque terms which incorporate the two mechanisms; adiabatic and non-adiabatic torques, respectively. The non-adiabatic constant β is chosen as 0.04 in

Table 1. Table representing the equilibrium positions of HH-U and HH-D at an anti-notch of different widths from $W_{AN} = 80$ to 140 nm at a fixed height of $H_{AN} = 200$ nm.

Anti notch width W_{AN}		
80 nm		
100 nm		
120 nm		
140 nm		

our simulations. The effective drift velocity of the conduction electron spins (u) is defined by

$$u = J \frac{g\mu_B p}{2eM_s} \quad (2)$$

where J is the current density, p is the spin polarization which is assumed to be 0.7 in our simulations, μ_B is the Bohr magneton and e is the electron charge.

3. Results and discussion

3.1. Anti-notch and current density

To gain an insight into how the anti-notch affects the current flow through the nanowire, we modelled the structure using the COMSOL multiphysics modelling software. Shown in figure 1(b) is the current density distribution in a nanowire with

an anti-notch, $W_{AN} = 160$ nm and height $H_{AN} = 200$ nm. The current flows along the $+x$ direction (left to right) and the current density is $J = 10^{12}$ A m $^{-2}$. A similar modelling was carried out for different notch dimensions and current densities. Our results reveal that current flows only through the nanowire with a negligible amount into the anti-notch. In all our micromagnetic simulations, the current distribution through the wire was set to be the same as that obtained from COMSOL.

3.2. Pinning of the DW at anti-notch

3.2.1. Anti-notch width variation. In this section, we investigate the effect of the anti-notch width on the motion of current-driven transverse DWs in Ni $_{80}$ Fe $_{20}$ nanowires. The anti-notch width, W_{AN} , is varied from 40 to 200 nm, while the anti-notch height, H_{AN} , is kept at 200 nm. The DWs are driven from left to right along the $+x$ direction in the nanowire. From our simulation on a nanowire without defects, the Walker breakdown is observed when the effective conduction electron drift velocity $u = 80$ m s $^{-1}$. For all our simulations, we use a conduction electron drift velocity of $u = 70$ m s $^{-1}$, which corresponds to a current density of $J = 1.48 \times 10^{12}$ A m $^{-2}$ for our wire geometry. Shown in figure 2 are the equilibrium DW positions for HH-U and HH-D at an anti-notch geometry with $W_{AN} = 40$ nm. For HH-U, the DW is stable beneath the anti-notch structure, whereas for HH-D, the DW is pushed away to a distance E_P from the centre of the anti-notch structure, as seen in figure 2(b). This difference in equilibrium position is due to the potential seen by the respective DWs at the anti-notch. For HH-U, the anti-notch acts as a potential well, whereas for HH-D the anti-notch is seen as a potential barrier. This implies that the potential at the anti-notch as seen by the DW is dependent on the chirality of the DW.

Interestingly, a completely different behaviour is observed when $W_{AN} = 120$ nm. The equilibrium positions of the DWs are shown in figure 3. As seen from figure 3(a), there is a change in the type of the potential disruption seen by the DW at the anti-notch. The anti-notch acts as a potential barrier for HH-U and a potential well for HH-D. This implies a change in the potential landscape of the anti-notch with varying width. To gain a better understanding of the DW interaction with the notch, we show the equilibrium positions of the DW at various anti-notch widths in table 1. We note that the transformation in the potential landscape occurs when the anti-notch width $W_{AN} = 100$ nm. The change in the potential polarity of the anti-notch can be explained by the transformation in the orientation of the spins along the anti-notch. For an anti-notch width of $W_{AN} \leq 100$ nm, the magnetization state within the anti-notch prefers to align parallel to the y -direction to minimize the demagnetizing energy as induced by shape anisotropy. This magnetic configuration within the anti-notch leads to the formation of magnetic charges oriented in the y -direction, as depicted in the inset of figure 2(a). These magnetic charges explain the different potential as seen by the HDDW with different transverse components. From figure 2(a) we can clearly observe that when the HH-U reaches the anti-notch, the transverse spins within the DW are aligned

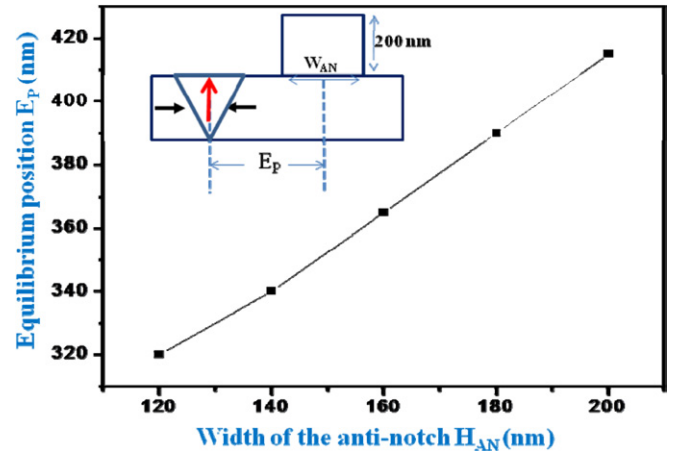


Figure 4. The equilibrium position of HH-U from the centre of the anti-notch as a function of the width of the anti-notch at a fixed height of 200 nm.

in the same direction as the spins in the anti-notch. The magnetic charges are of opposite polarity, as seen in the inset of figure 2(a), which leads to the attraction of the DW beneath the anti-notch to minimize the demagnetizing energy. Conversely, for the HH-D, the transverse spins of the DW are aligned in the opposite direction with the spins of the anti-notch, leading to a case where magnetic charges are of the same polarity, as seen in the inset of figure 2(b). This results in the repulsion between the same magnetic charges giving rise to the formation of a potential barrier for HH-D. Similar results were observed in the case of field-induced DW motion at the anti-notch geometry [9].

For $W_{AN} > 100$ nm, we observed a change in the polarity of the potential as seen by the DWs at the anti-notch. This is due to the decrease in the demagnetization factor along the x -direction in the anti-notch. The magnetization direction is no longer constrained to the y -direction. The spins within the anti-notch have a preferential alignment along the x -direction, adopting the magnetization direction of the nanowire. The transverse components of the DW are now aligned orthogonally to the magnetization in the anti-notch. This leads to the repulsion of the HH-U, due to the interaction of the positive charges from both the DW and the anti-notch. The DW is pushed to a distance E_P away from the centre of the anti-notch. For the HH-D, the opposite charge leads to the attraction of the DW within the notch, trapping the DW at the left edge of the anti-notch.

Additionally, when the anti-notch acts as a barrier, the DW undergoes a damped oscillation prior to reaching the equilibrium position. Figure 4 shows the variation of the equilibrium position of HH-U from the centre of the anti-notch ($W_{AN} > 100$ nm) with increasing anti-notch width. The equilibrium position moves far from the anti-notch with increasing anti-notch width. The increase in the distance between the anti-notch and the HH-U is attributed to the increase in the potential of the anti-notch with increasing width. When the anti-notch acts as a potential barrier for the HH-D ($W_{AN} \leq 100$ nm), the equilibrium position is almost stable at all widths, which is around 70 nm away from the left edge of

Table 2. Table representing the type of potential disruption observed by the DW at an anti-notch of different heights and widths. All the heights and widths are in nm. DW chiralities shown in table are HH-U and HH-D.

Height Width	Chirality	100 nm	150 nm	200 nm	250 nm	300 nm
40 nm		Well	Well	Well	Well	Well
		Barrier	Barrier	Barrier	Barrier	Barrier
60 nm		Barrier	Well	Well	Well	Well
		Well	Barrier	Barrier	Barrier	Barrier
100		Barrier	Barrier	Well	Well	Well
		Well	Well	Barrier	Barrier	Barrier
120 nm		Barrier	Barrier	Barrier	Well	Well
		Well	Well	Well	Barrier	Barrier
140 nm		Barrier	Barrier	Barrier	Barrier	Well
		Well	Well	Well	Well	Barrier
160 nm		Barrier	Barrier	Barrier	Barrier	Barrier
		Well	Well	Well	Well	Well

the anti-notch. This shows that there is no significant change in the potential of the anti-notch with the variation of the width when $W_{AN} \leq 100$ nm.

3.2.2. Anti-notch height variation. In this section we have investigated the effect of the anti-notch height on the

motion of the current-driven transverse DW in the $Ni_{80}Fe_{20}$ nanowire. The anti-notch height was varied from $H_{AN} = 100$ to 300 nm at different widths ranging from $W_{AN} = 40$ nm to $W_{AN} = 160$ nm. The results obtained from our micromagnetic simulations are summarized in table 2. Our results show that an anti-notch of heights from $H_{AN} = 100$ to 300 nm acts as

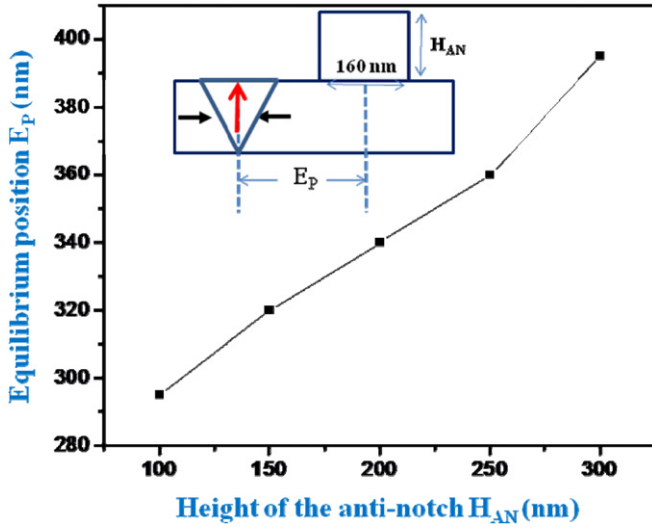


Figure 5. The equilibrium position of HH-U from the centre of the anti-notch as a function of the height of the anti-notch at a fixed width of 160 nm.

a potential well for HH-U and a potential barrier for HH-D at an anti-notch width $W_{AN} = 40$ nm. Conversely, it acts as a potential barrier for HH-U and a potential well for HH-D when anti-notch width $W_{AN} = 160$ nm. However, as the height of the anti-notch changes from $H_{AN} = 100$ to 300 nm, a transition in the polarity of the potential is observed at increasing widths from $W_{AN} = 60$ to 140 nm. By a careful observation of the potential disruption variation with the dimensions of the anti-notch, the transition in the potential polarity is seen at an anti-notch H_{AN}/W_{AN} ratio of 2. The transition in the potential behaviour of the anti-notch is due to the change in the relative orientation between the spins in the anti-notch and the nanowire. For $H_{AN}/W_{AN} < 2$, the spins in the anti-notch and the wire run almost parallel to each other. However, in the case of $H_{AN}/W_{AN} \geq 2$, the spins in the anti-notch and the wire are orthogonal to each other. When $H_{AN}/W_{AN} < 2$, the magnetic charges at the HH-U and the anti-notch are of the same polarity, which causes repulsion, resulting in a potential barrier at the anti-notch. When $H_{AN}/W_{AN} \geq 2$, the magnetic charges at the HH-U and the anti-notch are of opposite polarity, which causes attraction between them, resulting in a potential well at the anti-notch. Similar but opposite behaviour is observed in the case of HH-D. The equilibrium positions from the centre of the anti-notch are calculated when anti-notch acts as a barrier for HH-U and HH-D. The variation of the equilibrium position of HH-U with the anti-notch height is presented in figure 5. The plot shows that the equilibrium position of HH-U moves away from the centre of the anti-notch as the height of the anti-notch increases. This is attributed to the increase in the potential with the height of the anti-notch for HH-U when $H_{AN}/W_{AN} < 2$. However, in the case of HH-D, the equilibrium position of the DW is almost stable with varying height. This stable behaviour shows that the potential barrier is constant with varying height of the anti-notch for HH-D when $H_{AN}/W_{AN} \geq 2$.

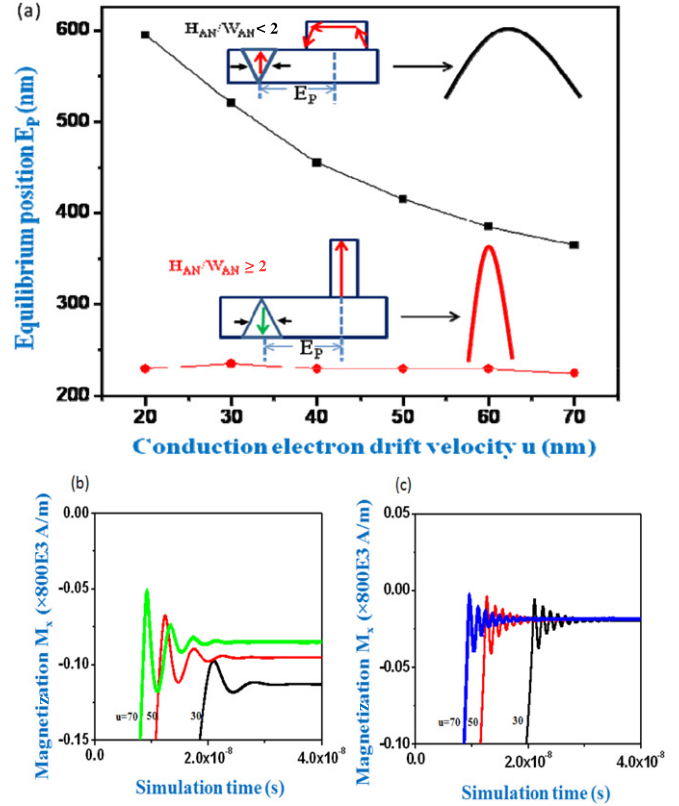


Figure 6. (a) The equilibrium position of HH-U and HH-D from the centre of the anti-notch as a function of the current density. (b) DW damped oscillations in magnetization as a function of simulation time for HH-U at various current densities. (c) DW damped oscillations in magnetization as a function of simulation time for HH-D at various current densities.

3.3. Variation of the potential with varying current density

The equilibrium position of the DW from an anti-notch is calculated by varying the current density u from 20 to 70 m s^{-1} when the anti-notch acts as a potential barrier for HH-U ($H_{AN}/W_{AN} < 2$) and HH-D ($H_{AN}/W_{AN} \geq 2$). The variation of the equilibrium positions of HH-U and HH-D with increasing current density is plotted in figure 6(a). For the anti-notch with $H_{AN}/W_{AN} < 2$, the equilibrium position of HH-U moves closer to the centre of the anti-notch as the current density is increased. However, for the anti-notch with $H_{AN}/W_{AN} \geq 2$, the equilibrium position of HH-D is almost constant with increasing current density. The DW undergoes damped oscillation prior to coming to an equilibrium position when the anti-notch acts as a barrier. Shown in figures 6(b) and (c) are the variation of the total magnetization of the structure with the simulation time at various current densities for HH-U and HH-D, respectively. The oscillation in the magnetization is due to the oscillation of the DW displacement. The time period of the damped oscillation decreases with increasing current density in the case of the anti-notch with $H_{AN}/W_{AN} < 2$ acting as a barrier, whereas it is constant in the case of $H_{AN}/W_{AN} \geq 2$. The decrease in the equilibrium position and the oscillation period with increasing current density is attributed to the smooth and gradual potential barrier at the anti-notch of $H_{AN}/W_{AN} < 2$. The constant equilibrium position

and oscillation period with increasing current density shows that the potential barrier is steep with an abrupt increase at the anti-notch of $H_{AN}/W_{AN} \geq 2$. It can be broadly understood that the potential barrier is smooth and gradual if the transverse spins of the wall are orthogonal to the notch configuration, whereas the barrier is abrupt and steep when the spins in the notch are anti-parallel to the transverse component.

4. Conclusion

In summary, the variation of the potential disruption observed by the DW at an anti-notch is studied as a function of DW chirality and anti-notch dimensions. Our results reveal that the potential disruption experienced at the anti-notch is a function of DW chirality. The polarity of the DW potential, either well or barrier, is strongly dependent on the anti-notch dimensions. A transition in the potential disruption at the anti-notch is observed at an anti-notch height-to-width ratio of 2. An increase in the DW equilibrium position for $H_{AN}/W_{AN} < 2$ shows an increase in the potential barrier with the height and width of the anti-notch. The constant equilibrium position of the DW for $H_{AN}/W_{AN} \geq 2$ shows that the potential barrier does not vary with the anti-notch dimensions. The variation of the equilibrium position and the damped oscillation time period with current density reveals that the potential barrier is smooth and gradual when spins in the anti-notch are orthogonal to the transverse component of the DW. The potential barrier is steep and abrupt when the spins in the anti-notch are aligned with the transverse component of the DW.

Acknowledgments

This work was supported in part by the NRF-CRP program (Multifunctional Spintronic Materials and Devices) and the Agency for Science, Technology and Research (A*STAR) SERC grant (082 101 0015).

References

- [1] Parkin S S P, Hayashi M and Thomas L 2008 *Science* **320** 190
- [2] Allwood D A, Xiong G, Faulkner C, Atkinson D, Petit D and Cowburn R P 2005 *Science* **309** 1688
- [3] Berger L 1984 *J. Appl. Phys.* **55** 1954
- [4] Zeng H T, Read D, O'Brien L, Sampaio J, Lewis E R, Petit D and Cowburn R P 2010 *Appl. Phys. Lett.* **96** 262510
- [5] McMichael R D and Donahue M J 1997 *IEEE Trans. Magn.* **33** 4167
- [6] Nakatani Y, Thiavelli A and Miltat J 2005 *J. Magn. Magn. Mater.* **290** 750
- [7] Hayashi M, Thomas L, Rettner C, Moriya R, Jiang X and Parkin S S P 2006 *Phys. Rev. Lett.* **97** 207205
- [8] Atkinson D, Eastwood D S and Bogart L K 2008 *Appl. Phys. Lett.* **92** 022510
- [9] Petit D, Jausovec A-V, Read D and Cowburn R P 2008 *J. Appl. Phys.* **103** 114307
- [10] Petit D, Jausovec A-V, Zeng H T, Lewis E, O'Brien L, Read D and Cowburn R P 2009 *Phys. Rev. B* **79** 214405
- [11] Klaui M *et al* 2005 *Appl. Phys. Lett.* **87** 102509
- [12] Petit D, Zeng H T, Sampaio J, Lewis E, O'Brien L, Jausovec A-V, Read D, Cowburn R P, O'Shea K J, McVitie S and Chapman J N 2010 *Appl. Phys. Lett.* **97** 233102
- [13] Hayward T J, Bryan M T, Fry P W, Fundi P M, Gibbs M R J, Im M Y, Fischer P and Allwood D A 2010 *Appl. Phys. Lett.* **96** 052502
- [14] Huang S-H and Lai C-H 2009 *Appl. Phys. Lett.* **95** 032505
- [15] Varga R, Garcia K L, Vázquez M and Vojtanik P 2005 *Phys. Rev. Lett.* **94** 017201
- [16] Varga R, Zhukov A, Blanco J M, Ipatov M, Zhukova V, Gonzalez J and Vojtanik P 2006 *Phys. Rev. B* **74** 212405
- [17] Varga R, Zhukov A, Usov N, Blanco J M, Gonzalez J, Zhukova V and Vojtanik P 2007 *J. Magn. Magn. Mater.* **316** 337
- [18] Himeno A, Kasai S and Ono T 2005 *Appl. Phys. Lett.* **87** 243108
- [19] OOMMF is available at <http://math.nist.gov>
- [20] OOMMF Extension for Current-induced Domain Wall Motion developed by IBM Research, Zurich; see <http://www.zurich.ibm.com/st/magnetism/spintevolve.html>